New Journal of Physics
The open-access journal for physics

N-doped ZnO thin films and nanowires: energetics, impurity distribution and magnetism

Qian Wang[1,2,4], **Qiang Sun**[2,3] **and Puru Jena**[2]

[1] School of Physical Science and Technology, Southwest University, Chongqing 400715, People's Republic of China
[2] Department of Physics, Virginia Commonwealth University, Richmond, VA 23284, USA
[3] Department of Advanced Materials and Nanotechnology, and Center for Applied Physics and Technology, Peking University, Beijing, People's Republic of China
E-mail: qwang@vcu.edu

New Journal of Physics **11** (2009) 063035 (14pp)
Received 16 March 2009
Published 19 June 2009
Online at http://www.njp.org/
doi:10.1088/1367-2630/11/6/063035

Abstract. Calculations based on density functional theory with generalized gradient approximation for exchange and correlation potential show that N-doped ZnO thin films and nanowires are magnetic. In neutral state, a total moment of 1 μ_B per N atom is introduced with 0.3–0.6 μ_B from N 2p orbitals. The mechanism contributing to magnetism in N-doped ZnO systems, however, is different from that in conventional transition metal-doped ZnO. Here magnetism is due to the holes in N 2p states induced by the substitution of oxygen with nitrogen. The N atoms show no tendency for clustering either on the ZnO thin film surfaces or on the NW surfaces, but they prefer the surface sites over the bulk sites. This study provides physical insight into the origin of magnetism in the new magnetic materials with no magnetic elements.

[4] Author to whom any correspondence should be addressed.

Contents

1. Introduction

Nitrogen, the most abundant element in the atmosphere, has rich chemistry. It is an important element in bio- and electronic materials. On the other hand, ZnO is a wide-band-gap semiconductor with novel magnetic, piezoelectric, electro-optic and electromechanical properties. Using N-doping to modify the properties of ZnO renders ZnO with multifunctional characteristics. For example, nitrogen has been considered as a suitable acceptor for making p-type ZnO [1]–[17] that can greatly improve the performance of ZnO-based optoelectronic devices. Since the ionic radius of N (0.75 Å) is nearly same as that of O (0.73 Å), N-doping can be expected to eliminate self-compensation effect [1]–[3], [5] arising from native defects such as oxygen vacancies and zinc interstitials. Thus, synthesis of N-doped p-type ZnO thin films has been hotly pursued: p-type ZnO films have been reported by using various deposition methods including molecular-beam epitaxy [2]–[4], chemical vapor deposition [5]–[9], sputtering [10]–[12], pulse laser deposition [13, 14], and thermal oxidation [15, 16]. In addition to the thin films, recently, high-quality ZnO nanowires (NWs) have been grown [17, 18] and well-aligned single-crystal p-type ZnO NW arrays were synthesized by using N_2O as a dopant via vapor–liquid–solid growth [19]. Thus, N-doped ZnO represents an important class of nanoscale building blocks for miniaturized electronic and optical devices.

Recently N-doped ZnO was found to be magnetic even without the presence of any traditional magnetic elements. Yu *et al* [20] prepared N-doped ZnO thin films using pulsed laser deposition and observed ferromagnetic (FM) behavior. They proposed a mechanism based on the picture of a Zn 3d hole produced by the compensation of the dangling bonds of nitrogen ions. In contrast, a recent theoretical study [21] found that the local magnetic moments are mainly localized on the 2p orbitals of doped N atoms instead of the 3d orbitals of Zn sites [20]. We note that the theoretical calculations [21] were carried out only for N-doped ZnO bulk phase. Therefore, one may wonder whether the observed magnetism in thin films is from 3d holes of Zn or from 2p orbitals of N sites because magnetism, in general, is quite sensitive to the geometry and to the local bonding environment. This is because bond lengths and coordination numbers, which are important parameters in magnetism, are different for thin films and bulk phase. Theoretical works [22]–[24] carried out thus far to explain the formation mechanism of p-type ZnO through N-doping are also only related to the bulk phase. While numerous experiments have focused on N-doped ZnO thin films [1]–[16], to the best of our knowledge, no theoretical work exists on N-doped ZnO thin films or NW systems. One of the reasons for this is the complicated surface reconstruction and the large supercells that are needed for modeling thin films with low doping concentration.

In this study, we have performed a first-principles study of the magnetic properties of N-doped ZnO thin films and NWs. We address the following issues: how much energy is needed to replace an O with N in ZnO thin films although N has a similar atomic radius as O? How are the N dopants distributed? What is the mechanism for making p-type ZnO through N-doping? How is ferromagnetism induced due to N-doping? In addition, our calculations of N-doped ZnO NWs enable us to study the effect of geometry and dimensionality on magnetism.

2. Computational method

Our study is based on spin-polarized density functional theory (DFT) with generalized gradient approximation (GGA) for exchange and correlation. We used the supercell approach where ZnO thin films along the $[11\bar{2}0]$ direction were modeled by (1×2) 9-layer and (2×2) 7-layer slab supercells having wurtzite structure. These contain a total of 36 and 56 formula units of ZnO, respectively. The central three layers of the slabs are kept frozen in their bulk positions, while the atoms on the top and bottom three (two) layers of the 9-layer (7-layer) slab were allowed to relax without any symmetry constraint. The surface layers of the top and bottom sides of the slabs were taken to be identical, which makes the thin film supercells central-symmetric. A vacuum region of 10 Å separated each slab from one another along the $[11\bar{2}0]$ direction. The slabs extend to infinity along the [0001] and $[1\bar{1}00]$ directions through periodic repetition of the supercell to mimic the large thin film surfaces in reality. A ZnO NW was generated from a $(7 \times 7 \times 2)$ ZnO bulk supercell having wurtzite structure by removing zinc and oxygen atoms from the outside area of a concentric cylinder with diameter of about 11.00 Å along the [0001] direction [25]. The NW supercell contains a total of 48 ZnO formula units and has a vacuum space of about 13 Å along the $[10\bar{1}0]$ and $[01\bar{1}0]$ directions. The length of the NW extends to infinity along the [0001] direction through supercell repetition. Nitrogen atoms with varying concentration were substituted at different O sites in ZnO as it has been found that N incorporates predominantly substitutionally at O sites [3].

The calculations of total energies, forces and optimization of geometries were carried out using a plane-wave basis set with the projector augmented plane wave (PAW) method [26] as implemented in the Vienna *ab initio* Simulation Package (VASP) [27]. The PW91 form [28] with the valence states $3d^{10}4s^2$ for Zn; $3p^34s^2$ for N; $2s^22p^4$ for O was used for the exchange and correlation potential. The cutoff energy was set at 420 eV for the plane-wave basis. For the (1×2) 9-layer slab supercell, we used $(6 \times 4 \times 1)$ and $(8 \times 6 \times 1)$ Monkhorst–Pack grid [29], respectively, for the structure optimization and for total energy and charge density calculations. For the (2×2) 7-layer supercell, $(5 \times 5 \times 1)$ and $(7 \times 7 \times 1)$ k-point meshes were selected. However, for the NW supercell, we chose $(1 \times 1 \times 6)$ and $(1 \times 1 \times 8)$ Monkhorst–Pack grid, respectively, due to the large vacuum space along both the $[10\bar{1}0]$ and $[01\bar{1}0]$ directions. In all the calculations, self-consistency was achieved with a tolerance in the total energy of 10^{-4} eV. Hellman–Feynman force components on each ion in the supercells were converged to 0.001 eV $Å^{-1}$. It was verified that the thickness of the slabs and the vacuum space are adequate to study the effects of surface [30, 31]. The $[11\bar{2}0]$ surface reconstruction and the reliability of our calculations have been well established from our previous work [32, 33]. The calculated binding energies for O_2 and N_2 are -5.625 and -9.586 eV, respectively, while the O–O and N–N bond lengths are 1.223 and 1.120 Å, respectively, which are in good agreement with the experimental values of 1.220 and 1.098 Å [34].

The formation energy for N substitution (N_O) represents the energy cost for substituting an O atom with N in neutral state ZnO and is calculated by using the following formula [23, 25]:

$$E_f(N_O) = (E^N_{tot} - E^0_{tot} + n\mu_O - n\mu_N)/n, \quad (1)$$

where E^N_{tot} is the total energy of the supercell containing nitrogen atoms, E^0_{tot} is the total energy of the pure ZnO supercell, n is the number of O atoms replaced by N atoms, and μ_O and μ_N are the chemical potentials of oxygen and nitrogen atoms, respectively. We note that the chemical potentials μ_j (j = Zn, O and N) depend on the experimental growth conditions and the designated source. The μ_O and μ_{Zn} have upper limits given by the energy of O in an O_2 molecule and the energy of zinc in hexagonal close-packed bulk, which correspond to O-rich conditions and Zn-rich conditions (lower limit of O-poor conditions), respectively. Similarly, when the source gas is N_2, we have $\mu_N = \frac{1}{2}\mu_{N_2}$. When the source gas is N_2O, we have $\mu_N = \frac{1}{2}\mu_{N_2O} - \mu_O$. The range of ambient O from O-poor to O-rich is subject to the magnitude of the formation enthalpy of ZnO, ΔH(ZnO). In thermodynamic equilibrium, $\Delta H(\mathrm{ZnO}) = \mu_O + \mu_{Zn}$, which is calculated to be −3.42 eV, close to the experimental value of −3.6 eV [35]. In all calculations, the atomic coordinates of all the atoms (except for those in the central layers of the slabs, which were fixed in their bulk positions) were relaxed without any symmetry constraint, and all the calculations were carried out in the conditions of Zn-rich and N_2 being source gas to ensure effective N-doping.

3. Results and discussion

We begin our discussions with the (1 × 2) 9-layer ZnO slab. To study the site preference of N we first replaced one O atom belonging to the surface, subsurface and bulk-like site with one N atom on the top half of the slab (see figure 1 (C_{11})–(C_{13})). The corresponding sites on the bottom half of the slab are also replaced to preserve symmetry. This led to a $Zn_{36}N_2O_{34}$ supercell with N-doping concentration of 5.56%. It was found that the surface site, configuration C_{11}, is lower in energy than configurations C_{12} and C_{13} by 0.05 and 0.407 eV, respectively. The calculated results are given in table 1. The formation energy of N_O is found to be 2.894 eV N^{-1} for configuration C_{11}. The average Zn–N bond length is 1.911 Å and shows no significant change from that of the calculated surface Zn–O bond length (1.917 Å) without N. This is because of the similar sizes of O and N atoms. For configurations C_{12} and C_{13}, the formation energies are found to be 2.905 and 3.098 eV N^{-1}, which are 0.011 and 0.204 eV higher, respectively, than that in configuration C_{11}, signifying that configurations C_{11} and C_{12} are nearly energetically degenerate. The Zn–N bond lengths are 1.941 and 1.978 Å for N at the subsurface and the bulk-like sites, respectively. These indicate that formation of the N_O on the surface and subsurface sites is easier than that in the bulk-like sites.

More interestingly, we note that the calculated total magnetic moments for all the configurations (C_{11}–C_{13}) in N-doped ZnO are about 2.000 μ_B (see table 1). This implies that replacing one O with one N induces a moment of 1.000 μ_B. To further investigate the origin and distribution of this magnetic moment, we calculated the magnetic moment on each atom for these configurations. We found that the magnetic moments on N atoms are 0.628, 0.415 and 0.391 μ_B in C_{11}, C_{12} and C_{13}, respectively, and they mostly arise from the N 2p orbitals (0.611, 0.400 and 0.372 μ_B) with negligible contributions from N 2s (0.017, 0.015 and

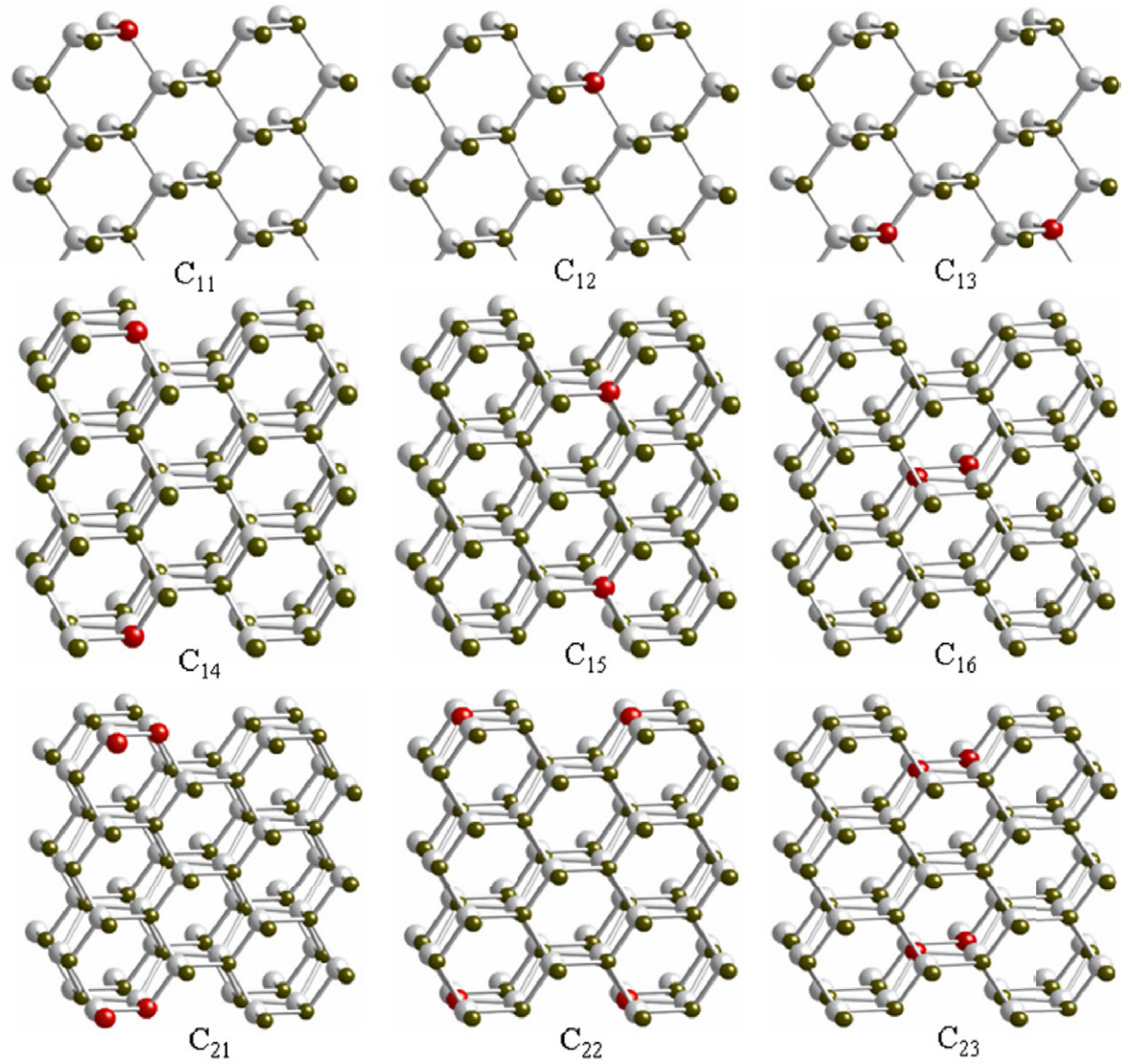

Figure 1. Schematic representation of the non-equivalent configurations of N replacing O sites in the $Zn_{36}O_{36}$ (the lower part of the slab is not shown) and $Zn_{56}O_{56}$ slab supercells for thin films. The darker (dark green) and smaller spheres, lighter (light gray) and bigger spheres, and dark (red) spheres represent O, Zn and N atoms, respectively.

0.019 μ_B, respectively). The neighboring Zn and O atoms are polarized and carry a small moment of about 0.020–0.045 μ_B. The calculated local moment on the N atom in the bulk-like site (configuration C_{13}) is comparable to that in the bulk sites (0.4 μ_B) obtained in previous theoretical study [21]. It is understandable that replacing one O with N in ZnO introduces a magnetic moment of 1 μ_B as the electronic configurations of N and O atoms are, respectively, $1s^2 2s^2 2p^3$ and $1^2 2s^2 2p^4$, i.e. N atom has one valence electron less than O atom. The substitution of O with N leads to holes in N 2p states which form local magnetic moments and result in p-type ZnO.

Table 1. Formation energy of nitrogen $E_f(N_O)$ (in eV), total magnetic moment M_{total} (in μ_B) per supercell, local moment on nitrogen atom M_N (in μ_B) resulting from the replacement of oxygen with nitrogen, and the average Zn–N bond length for the N-doped ZnO thin film configurations shown in figure 1.

Configurations	$E_f(N_O)$	M_{total}	M_N	d_{Zn-N}
C_{11}	2.894	1.997	0.628	1.911
C_{12}	2.905	2.000	0.415	1.941
C_{13}	3.098	2.000	0.391	1.978
C_{14}	2.844	2.000	0.633	1.910
C_{15}	2.898	2.000	0.417	1.945
C_{16}	3.031	2.000	0.390	1.978
C_{21}	2.901	3.999	0.553	1.910
C_{22}	2.922	3.997	0.517	1.908
C_{23}	2.926	4.000	0.406	1.945

However, due to the hybridizations between the N and the neighboring Zn and O atoms, the local moment is reduced dissimilarly depending on the site the N atom occupies. The different values of the local moments on different N sites are attributed to the different bonding environment. For instance, there are four Zn–N bonds when N atom occupies the subsurface or bulk-like sites, whereas there are only three Zn–N bonds when N atom is on the surface layer. Compared with the three-fold-coordinated surface sites, the four-fold-coordinated subsurface and bulk-like sites have reduced atomic moment on N sites due to enhanced orbital hybridization.

To confirm that the calculated magnetic properties are not a consequence of the specific supercell construction or nitrogen concentration, we generated a larger (2×2) 7-layer supercell having $[11\bar{2}0]$ surface orientation and containing a total of 112 ZnO atoms ($Zn_{56}O_{56}$). We replaced one O atom with N on either side of the slab at different sites (configurations C_{14}–C_{16} in figure 1) leading to a N_O concentration of 3.6%. We found that the energy corresponding to configuration C_{14} is lower from those of C_{15} and C_{16} by 0.091 and 0.370 eV, respectively. This again indicates that N prefers the surface sites over the bulk-like sites. The N_O formation energies are calculated to be 2.844, 2.898 and 3.031 eV, respectively, for configurations C_{14}–C_{16}. Once again, we note that the replacement of two O atoms with N introduces a total moment of 2.000 μ_B in the surpercell for all the configurations irrespective of where N atoms reside. The local moments on N sites are found to be 0.633, 0.417 and 0.390 μ_B for configurations C_{14}–C_{16}, respectively, and mainly come from the N 2p orbitals. The results are given in table 1. We see that the N_O formation energies are slightly smaller than those in similar configurations in the 9-layer slab. Thus, we have verified that the site preference and the magnetic moment of N in N-doped ZnO thin films are not affected by supercell construction or N concentration.

In figures 2(a)–(d), we plot the electronic density of states (DOS) corresponding to the ground state configuration C_{14}. The dotted line indicates the Fermi energy. For comparison we also plot the total spin DOS and the partial DOS of Zn and O for pure $Zn_{56}O_{56}$ supercell in figures 2(a), (c) and (d), respectively, which show that the spin-up and spin-down DOS are totally symmetric and hence lead to zero magnetic moment. The energy gap between the valence band maximum (VBM) and the conduction band minimum is large exhibiting the

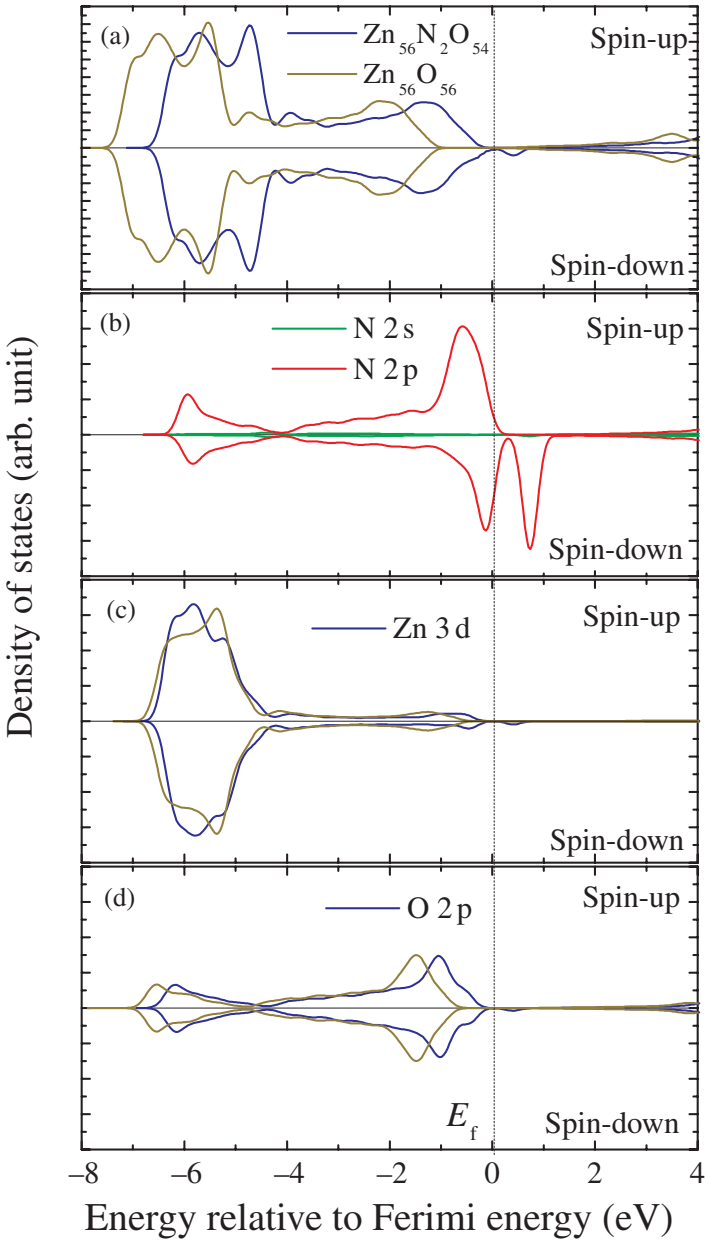

Figure 2. (a) Calculated total spin DOS, (b) partial DOS of N, (c) and (d) partial DOSs, respectively, at Zn and O adjacent to the N atom in $Zn_{56}N_2O_{54}$. The lighter (dark yellow) lines in (c) and (d) correspond to partial DOSs of Zn 3d and O 2p for the pure ZnO supercell, respectively.

semi-conducting feature of ZnO thin films. When N atoms are incorporated into ZnO, new states are introduced above the VBM and the energy gap is reduced, suggesting that N-doping can improve electronic conductivity. The 2p orbitals of N are spin polarized (see figure 2(b)), resulting in an asymmetric spin-up and spin-down DOS (figure 2(a)) and making the system magnetic. On the neighboring O sites, the O 2p orbitals are slightly polarized (see figure 2(c)), but 3d orbitals of Zn are almost unchanged and make negligible contribution to the moment (see figure 2(d)). Therefore the observed magnetism is primarily from N 2p orbitals.

To further study the effect of the concentration and distribution of N_O on the ferromagnetism, we replaced a pair of O atoms with N on either side of the (2×2) slab with different N–N distances. This corresponds to a N concentration of 7.14%. Three different configurations C_{21}–C_{23} as shown in figure 1 were studied. All configurations exhibit FM coupling, each with a total magnetic moment of about $4.000\,\mu_B$. The moments at the N site range from 0.406 to $0.553\,\mu_B$ and are predominately contributed by N 2p orbitals. Configuration C_{21} was found to be lower in energy than those of C_{22} and C_{23} by 0.021 and 0.036 eV, respectively. These can be regarded as energetically degenerate. Therefore, N_O can be distributed homogeneously in the surface and subsurface layers of ZnO thin films. The formation energies of N_O in these configurations are found to be a little bit larger than those for the configurations with lower N concentration (see table 1). Thus, we confirm that the calculated properties of N-doped ZnO are independent of the supercell size or the N-doping concentration.

We then studied the magnetic interaction between the two N atoms and the stability of the FM state versus antiferromagnetic (AFM) state. We calculated the total energies corresponding to both FM ($N_{O_1}\uparrow$, $N_{O_2}\uparrow$) and AFM ($N_{O_1}\uparrow$, $N_{O_2}\downarrow$) spin alignments for configurations $C_{21} - C_{23}$. The $N_O\uparrow$ and $N_O\downarrow$ stand for spin-up and spin-down states, respectively, The preferred magnetic coupling is determined by comparing the energy difference between the FM and AFM states, namely, $\Delta E^{mag} = E_{AFM}(N_{O_1}\uparrow\ N_{O_2}\downarrow) - E_{FM}(N_{O_1}\uparrow\ N_{O_2}\uparrow)$. For the ground state configuration C_{21}, it was found that the FM state is 82 meV lower in energy than the AFM state, which is sufficient to overcome thermal fluctuations to provide robust FM behavior. This is in agreement with experiment [18]. For the remaining two higher energy configurations C_{22} and C_{23}, the energy difference ΔE^{mag} is found to be 8 and 108 meV, respectively. Note the N–N distance in configuration C_{22} is large, namely 5.890 Å and hence the magnetic coupling is weak. The spin density distribution for the FM ground state of C_{21} is plotted in figure 3(a), which clearly shows that most of the spin density in the N-doped ZnO thin film is located on N 2p orbitals with a small contribution from the neighboring O and Zn atoms. Thus, we confirmed the local magnetic moments primarily arise from the N 2p orbitals instead of Zn 3d orbitals. The charge density distribution of the two N atoms in the surface layer is given in figure 3(b). We see an overlap between charge densities on Zn and N sites, which drives the coupling to be FM.

We finally extended our investigation of ZnO thin films to ZnO NWs and study the effect of geometry and dimensionality on the electronic and magnetic properties of N-doped ZnO as one can expect that the larger surface to volume ratio and curvature of the NW surface may enhance its magnetic properties. We constructed a NW supercell of $Zn_{48}O_{48}$. To study the dependence of energetics, distribution of the dopants, and magnetic coupling as a function of dopant concentration we have investigated twelve different configurations, as shown in figure 4. Configurations NW_{11}–NW_{13} correspond to replacing one O atom with N at the surface, subsurface and bulk-like sites of the NW surpercell. Configurations NW_{21}–NW_{25} represent the replacements of two O atoms by N at the surface sites with the closest distance (NW_{21}) and with the furthest separation distance (NW_{22}), one N at surface site and another one at subsurface site (NW_{23}), one at surface site and another at interior site (NW_{24}), and two N atoms at interior bulk-like sites with the closest distance (NW_{25}). Configurations NW_{31}–NW_{34} are achieved by replacing three O atoms with N at different surface and subsurface sites with different separation distances and directions. In table 2, we summarize the main results of our calculations of $Zn_{48}N_xO_{48-x}$ ($x = 1$, 2 and 3, corresponding to the doping concentration of 2.08, 4.17 and 6.25%, respectively).

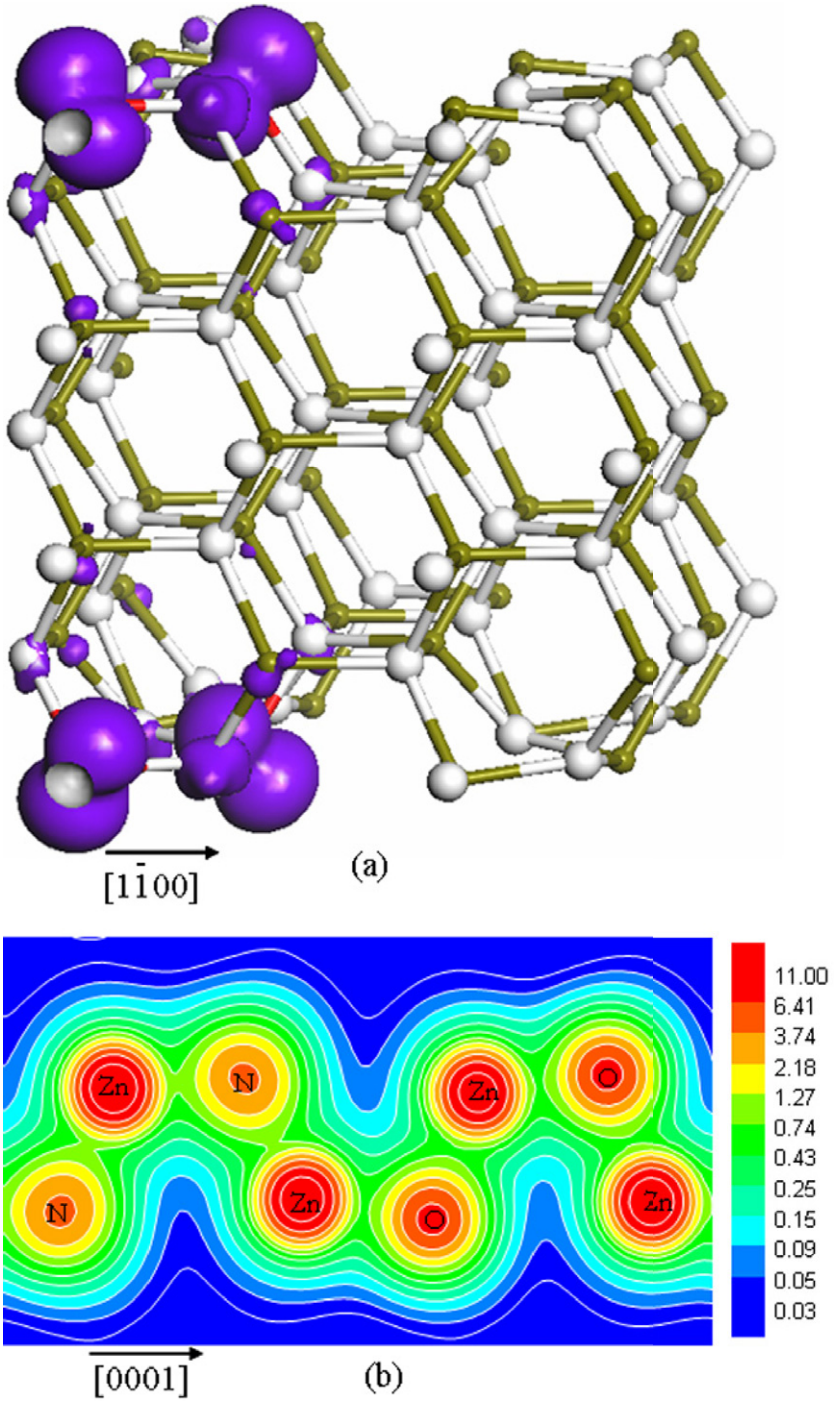

Figure 3. (a) Spin density distribution and (b) charge density distribution in the plane containing two N atoms and neighboring Zn and O atoms in the ground state of $Zn_{56}N_4O_{54}$ slab supercell.

We note that N atom energetically prefers the surface and subsurface sites over the interior sites and the N_O formation energies of configurations NW_{11} and NW_{12} are lower than that for NW_{13} by 0.305 and 0.214 eV N^{-1}, respectively. When two N atoms are substitutionally introduced to the NW, the formation energy of N_O is found to be insensitive to the dopant

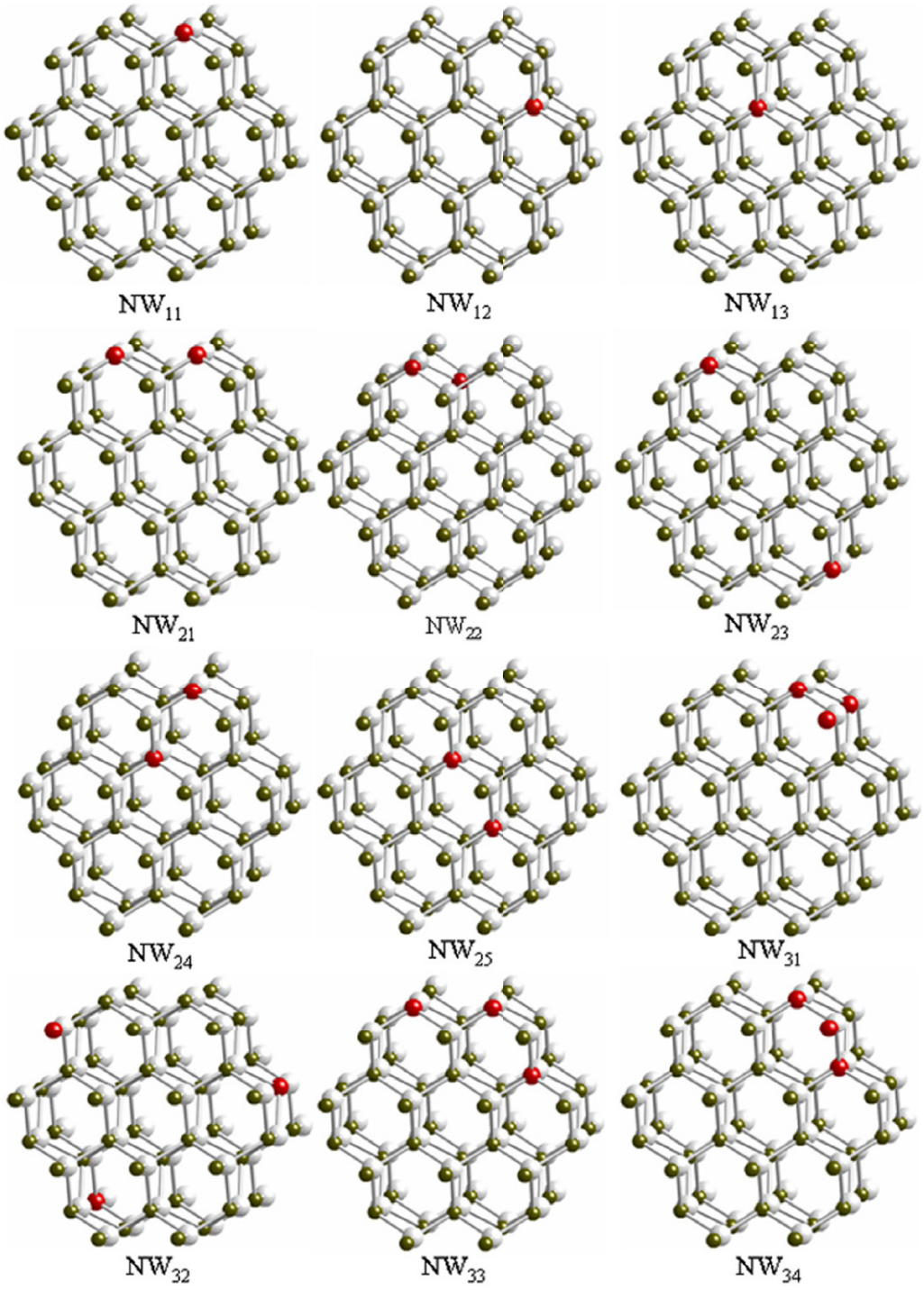

Figure 4. Schematic representation of the nonequivalent configurations of N-doping in the $Zn_{48}O_{48}$ nanowire supercell. The darker (dark green) and smaller spheres, lighter (light gray) and bigger spheres, and dark (red) spheres represent O, Zn and N atoms, respectively.

Table 2. Formation energy of nitrogen $E_f(N_O)$ (in eV), total magnetic moment M_{total} (in μ_B) per supercell, local moment on each nitrogen atom MN (in μ_B), and the average Zn–N bond length for different configurations shown in figure 4, for $Zn_{48}N_xO_{48-x}$ NW supercell. The N concentration (N at.%) is given in the first column.

Configurations	$E_f(N_O)$	M_{total}	M_N	d_{Zn-N}
C_{11}(2.08%)	2.884	1.000	0.510	1.907
C_{12}(2.08%)	2.975	1.000	0.394	1.951
C_{13}(2.08%)	3.189	1.000	0.308	1.991
C_{21}(4.17%)	2.999	2.000	0.510 0.510	1.914
C_{22}(4.17%)	2.993	2.000	0.510 0.510	1.907
C_{23}(4.17%)	2.997	2.000	0.561 0.390	1.932
C_{24}(4.17%)	3.008	2.000	0.561 0.312	1.952
C_{25}(4.17%)	3.022	2.000	0.315 0.315	1.988
C_{31}(6.25%)	2.978	3.000	0.537 0.554 0.491	1.910
C_{32}(6.25%)	2.998	3.000	0.512 0.512 0.512	1.908
C_{33}(6.25%)	2.909	3.000	0.569 0.558 0.417	1.932
C_{34}(6.25%)	2.882	3.000	0.575 0.529 0.420	1.927

separation distance on the NW surface, as configurations NW_{21}, NW_{22} and NW_{23} are nearly energetically degenerate. This shows that N dopants can be homogeneously distributed on the surface of the NW. The energy cost is larger to form N_O in NW_{24} and NW_{25} configurations. However, when three N atoms are incorporated, the distribution of N_O changes. Configuration NW_{34} where the three N atoms are in the nearest neighboring sites lies lower in energy by 0.285, 0.343 and 0.093 eV than configurations NW_{21}, NW_{22} and NW_{23}, respectively. This indicates that N atoms have a tendency to cluster when N_O reaches high concentration in the NW. Note, in experiments [1]–[16], [19, 20] the concentration of N_O is lower than 6.25%. Thus, clustering should not play a role in observed magnetism in N-doped ZnO systems. We found that the electronic structure of the N-doped ZnO NW shares some resemblance with that of the thin film surface as the total DOS and partial DOS of N, Zn and O around Fermi level are quite similar to each other. Of further note, the NW is magnetic with total magnetic moment of 1.000, 2.000 and 3.000 μ_B, respectively, when one, two and three O atoms are, respectively,

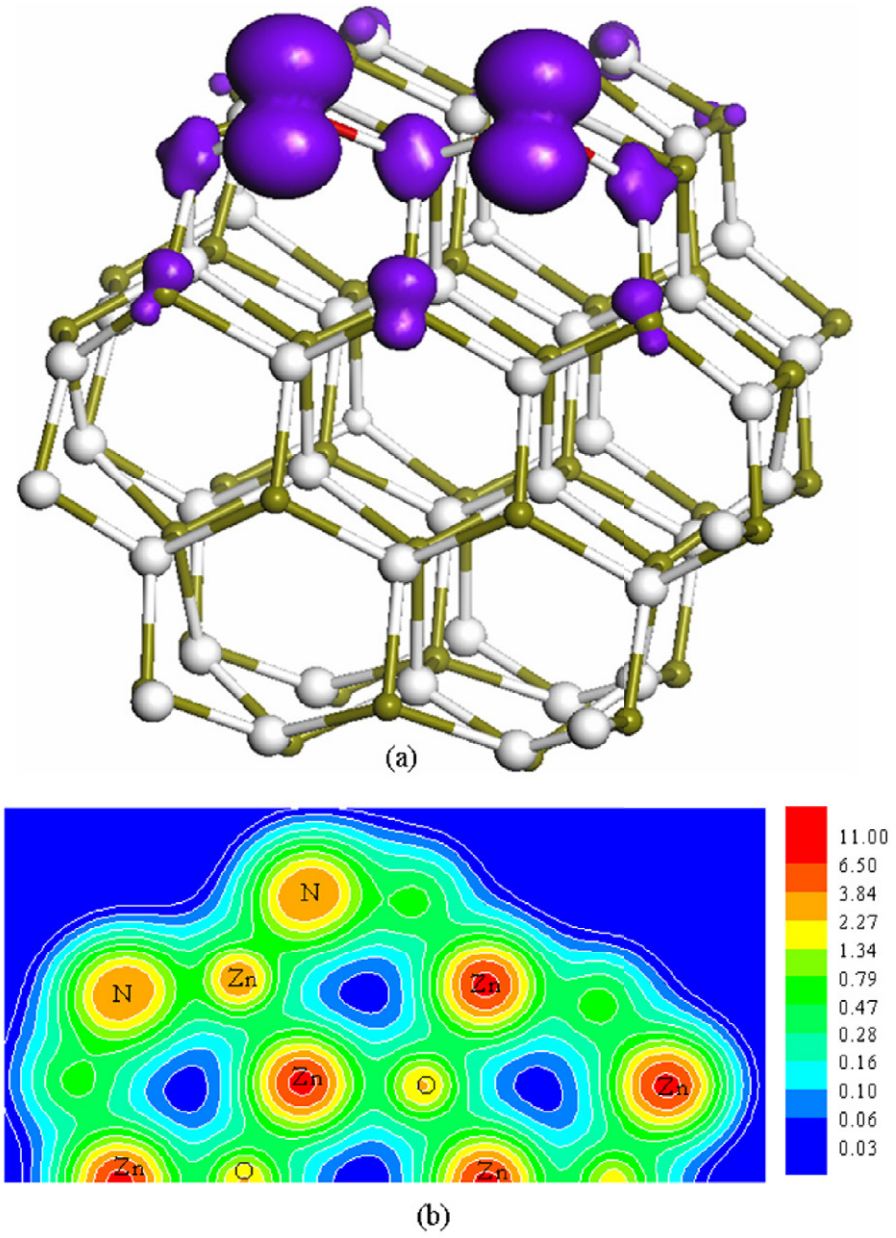

Figure 5. (a) Spin density distribution and (b) charge density distribution in the plane containing two N atoms and neighboring Zn and O atoms in the ground state of $Zn_{48}N_2O_{46}$ NW supercell.

replaced with N. For the surface shell sites, the N atoms carry a magnetic moment of about 0.510–0.575 μ_B, while in bulk-like sites or subsurface shell sites, the moment is reduced to 0.308–0.420 μ_B. Figures 5(a) and (b) show the calculated spin density distributions and charge density distributions for configuration NW_{21}, respectively. The large spatial extension of the N 2p spin states and the interaction between the N atoms and their neighboring atoms can be clearly seen in these two figures.

4. Summary

In summary, extensive calculations were carried out to understand the magnetic properties of N-doped ZnO thin films and NWs in neutral state. We show that N atoms prefer to occupy the surface sites. The substitution of oxygen by nitrogen leads to local magnetic moments with each N introducing a magnetic moment of 1.0 μ_B. The moments on the N sites range between 0.308 and 0.633 μ_B, depending upon the sites they occupy. The local magnetic moments mainly arise from the N 2p orbitals instead of Zn 3d orbitals, and couple ferromagnetically with each other. The origin of magnetism from N 2p orbitals has its roots in the atomic properties of nitrogen. N^{2-} has one electron less than O^{2-}, and the N 2p states have lower binding energy than O 2p states, forming a relatively narrow impurity band with one hole per N. The resulting holes in N 2p orbitals lead to the spin moments and make the systems magnetic. The induced magnetism is found to be stronger than that in the bulk phase [21] due to the reduced coordination in the surface of thin films and NWs. Our results are in agreement with recently observed magnetism in N-doped ZnO thin films [20]. The magnetism induced by N-doping opens a possible path to a new class of magnetic semiconductors whose properties are solely determined by the interactions between the holes in N 2p orbitals. Because N is an essential component of proteins, nucleic acids, vitamins and hormones that make life possible, and ZnO is biocompatible, N-doped ZnO may have interesting applications in biotechnology.

Acknowledgment

This work is partially supported by grants from the US Department of Energy and the National Natural Science Foundation of China (NSFC-10744006 and NSFC-10874007).

References

[1] Kobayashi A, Sankey O F and Dow J D 1983 *Phys. Rev.* B **28** 946
[2] Oh D C, Kim J J, Makino H, Hanada T, Cho M W, Yao T and Ko H J 2005 *Appl. Phys. Lett.* **86** 042110
[3] Fons P, Tampo H, Kolobov A V, Ohkubo M, Niki S and Tominaga J 2006 *Phys. Rev. Lett.* **96** 045504
[4] Lee C, Park Y and Lim J 2007 *J. Korean Phys. Soc.* **50** 590
[5] Dunlop L, Kursumovic A and MacManus-Driscoll J L 2008 *Appl. Phys. Lett.* **93** 172111
[6] Zeng Y J, Ye Z Z, Lu Y F, Xu W Z, Zhu L P, Huang J Y, He H P and Zhao B H 2008 *J. Phys. D: Appl. Phys.* **41** 165104
[7] Du G, Ma Y, Zhang Y and Yang T 2005 *Appl. Phys. Lett.* **87** 213103
[8] Rommeluère J F, Svob L, Jomard F, Mimila-Arroyo J, Lusson A and Sallet V 2003 *Appl. Phys. Lett.* **83** 287
[9] Chen L L, Lu J G, Ye Z Z, Lin Y M, Zhao B H, Ye Y M, Li J S and Zhu L P 2005 *Appl. Phys. Lett.* **87** 252106
[10] Lu J G, Ye Z Z, Zhuge F, Zeng Y J, Zhao B H and Zhu L P 2004 *Appl. Phys. Lett.* **85** 3134
[11] Nakano Y, Morikawa T, Ohwaki T and Taga Y 2006 *Appl. Phys. Lett.* **88** 172103
[12] Tsukazaki A *et al* 2005 *Nat. Mater.* **4** 42
[13] Hirai M and Kumar A 2007 *J. Vac. Sci. Technol.* A **25** 1534
[14] Li B S, Liu Y C, Zhi Z Z, Shen D Z, Lu Y M, Zhang J Y, Fan X W, Mu R X and Henderson D O 2003 *J. Mater. Res.* **18** 8
[15] Kaminska E *et al* 2005 *Phys. Status Solidi* c **2** 1119
[16] Lee J, Ha J, Hong J, Cha S and Paik U 2008 *J. Vac. Sci. Technol.* B **26** 1696
[17] Yuan G D, Zhang W J, Jie J S, Fan X, Zapien J A, Leung Y H, Luo L B, Wang P F, Lee C S and Lee S T 2008 *Nano Lett.* **8** 2591

[18] Zhao Q X, Willander M, Morjan R E, Hu Q-H and Campbell E E B 2003 *Appl. Phys. Lett.* **83** 165
[19] Wang X D, Zhou J, Lao C S, Song J H, Xu N S and Wang Z L 2007 *Adv. Mater.* **19** 1627
[20] Yu C F, Lin T J, Sun S J and Chou H 2007 *J. Phys. D: Appl. Phys.* **40** 6497
[21] Shen L, Wu R Q, Pan H, Peng G W, Yang M, Sha Z D and Feng Y P 2008 *Phys. Rev.* B **78** 073306
[22] Yamamoto T and Katayama-Yoshida H 1999 *Japan. J. Appl. Phys.* **38** L166
[23] Yan Y F and Zhang S B 2001 *Phys. Rev. Lett.* **86** 5723
[24] Limpijumnong S, Li X N, Wei S H and Zhang S B 2006 *Physica* B **376** 686
[25] Wang Q, Sun Q, Chen G, Kawazoe Y and Jena P 2008 *Phys. Rev.* B **77** 205411
[26] Kresse G and Joubert J 1999 *Phys. Rev.* B **59** 1758
[27] Kresse G and Furthmüller J 1996 *Phys. Rev.* B **54** 11169
[28] Wang Y and Perdew J P 1991 *Phys. Rev.* B **44** 13298
[29] Monkhorst J and Pack J D 1976 *Phys. Rev.* B **13** 5188
[30] Wang Q and Jena P 2004 *Appl. Phys. Lett.* **84** 4170
[31] Wang Q, Sun Q, Jena P and Kawazoe Y 2005 *Appl. Phys. Lett.* **87** 162509
[32] Wang Q, Sun Q, Jena P, Hu Z, Note R and Kawazoe Y 2007 *Appl. Phys. Lett.* **91** 063116
[33] Wang Q, Sun Q, Rao B K and Jena P 2004 *Phys. Rev.* B **70** 052408
[34] Lide D R (ed) 2000 *Handbook of Chemistry and Physics* (Boca Raton, FL: CRC Press)
[35] Tuomisto F, Saarinren K, Look D C and Farlow G C 2005 *Phys. Rev.* B **72** 085206